RSC Advances

PAPER

View Article Online
View Journal | View Issue

Cite this: *RSC Adv.*, 2017, **7**, 19223

Photoluminescence tuning of $Ca_{8-x}Sr_xMgGd(PO_4)_7:Eu^{2+},yMn^{2+}$ phosphors for applications in white LEDs with excellent color rendering index

Jiaqi Long, Yuzhen Wang, Chaoyang Ma, Xuanyi Yuan, Wenfeng Dong, Ran Ma, Zicheng Wen, Miaomiao Du and Yongge Cao *

Received 23rd December 2016
Accepted 24th March 2017

DOI: 10.1039/c6ra28594e

rsc.li/rsc-advances

Two series of novel phosphors of green-yellow emitting $Ca_{8-x}Sr_xMgGd(PO_4)_7:Eu^{2+}$ and yellow-orange emitting $Sr_8MgGd(PO_4)_7:Eu^{2+},yMn^{2+}$ were successfully synthesized by a solid-state reaction. The crystal structures, photoluminescence (PL), PL excitation (PLE) spectra and decay times were investigated in detail. Upon excitation at 350 nm, the $Ca_4Sr_4MgGd(PO_4)_7:Eu^{2+}$ phosphor showed strong green emission centered at 513 nm, and the $Sr_8MgGd(PO_4)_7:Eu^{2+}$ phosphor showed strong yellow emission centered at 513 nm and 593 nm, and $Sr_8MgGd(PO_4)_7:Eu^{2+},Mn^{2+}$ showed strong orange emission centered at 510 nm and 616 nm. In addition, a standard warm white-light emitting single-phased phosphor of $Sr_8MgGd(PO_4)_7:Eu^{2+},Mn^{2+}$ with chromaticity coordinates (x, y), correlated color temperature (CCT) and Commission Internationale de l'Eclairage (CIE) coordinates of (0.4497, 0.3929), 2705 K, and 89.7 was realized *via* energy transfer between Eu^{2+} and Mn^{2+}. The energy transfer was demonstrated to be a resonant type dipole–quadrupole mechanism. Moreover, the obtained LED device exhibits an excellent color-rendering index (R_a = 97) at a correlated color temperature of 5651 K with the CIE coordinates (0.3290, 0.3410).

1. Introduction

In recent years, white lighting-emitting diodes (LEDs) have attracted much attention because of their applications in liquid crystal displays and solid-state lighting.[1,2] The presently-commercialized white LEDs, fabricated by combining a blue-emitting LED chip with the yellow-emitting garnet phosphor ($Y_3Al_5O_{12}:Ce^{3+}$) have played an important role in solid-state lighting in recent years.[3] They are characterized by cool white light with Commission Internationale de l'Eclairage (CIE) chromaticity coordinates of (0.292, 0.325), a correlated color temperature (CCT) of 7756 K, and poor color rendering indices (CRI, R_a) of 75.[4,5] Trichromatic white LEDs are considered to be useful to improve the CRI of white LEDs for their high color-rendering properties.[6] Nevertheless, different aging rate for each phosphor and the reabsorption of the blue light by red and green phosphors, will lead to low luminescence efficiency in such system.[7] Recently, white LEDs fabricated using near-ultraviolet chips (360–420 nm) coupled with a blend of yellow- and blue-emitting phosphors have exhibited favorable properties, including tunable CCTs, tunable CIE chromaticity coordinates, and excellent R_a values. To realize full-spectrum LEDs, therefore, it is important to develop new green-yellow-emitting and yellow-orange-emitting phosphors for near-UV LED applications.

Recently, whitlockite-type hosts, for example, $Ca_9Lu(PO_4)_7:Eu^{2+},Mn^{2+}$,[8] $Ca_8MgGd(PO_4)_7:Eu^{2+}$,[9] $Sr_8MgGd(PO_4)_7:Eu^{2+}$,[10] $Sr_9Mg_{1.5}(PO_4)_7:Eu^{2+}$,[11] and $Ca_8MgY(PO_4)_7:Eu^{2+},Mn^{2+}$ (ref. 12) have been reported for LED phosphors due to their outstanding luminescence properties as down-conversion phosphors.

To the best of our knowledge, the crystal structures and luminescence properties of color tunable $Ca_{8-x}Sr_xMgGd(PO_4)_7:Eu^{2+}$ green-yellow-emitting phosphor and $Sr_8MgGd(PO_4)_7:Eu^{2+},yMn^{2+}$ yellow-orange-emitting phosphor have not yet been reported in the literature. In this study, we investigated the luminescence properties of color tunable green-yellow-emitting $Ca_{8-x}Sr_xMgGd(PO_4)_7:Eu^{2+}$ and yellow-orange-emitting $Sr_8MgGd(PO_4)_7:Eu^{2+},Mn^{2+}$ phosphors. In addition, white-light near-UV LEDs possessing excellent CRI values and warm correlated color temperatures were fabricated using phosphor blends of blue-emitting $Sr_5(PO_4)_3Cl:Eu^{2+}$ and red-emitting $Sr_4Al_{14}O_{25}:Mn^{4+}$ with some green-emitting $Ca_4Sr_4MgGd(PO_4)_7:0.02Eu^{2+}$ or yellow-emitting $Sr_8MgGd(PO_4)_7:0.02Eu^{2+}$ or orange-emitting $Sr_8MgGd(PO_4)_7:0.02Eu^{2+},0.25Mn^{2+}$ and their optical properties were investigated.

Beijing Key Laboratory of Opto-electronic Functional Materials & Micro-Nano Devices, Department of Physics, Renmin University of China, Beijing 100872, China

2. Experimental section

2.1 Materials and synthesis

Polycrystalline phosphors with composition of $Ca_{8-x}Sr_x$-$MgGd(PO_4)_7$:$0.02Eu^{2+}$ and $Sr_{7.98}MgGd(PO_4)_7$:$0.02Eu^{2+}$,yMn^{2+} described in this work were prepared with a high-temperature solid-state reaction. Briefly, the constituent raw materials $SrCO_3$ (A. R., 99.9%), $CaCO_3$ (A. R., 99.9%), MgO (A. R., 99%), Gd_2O_3 (A. R., 99.99%), $MnCO_3$ (A. R., 99.9%), $NH_4H_2PO_4$ (A. R., 99%), and Eu_2O_3 (A. R., 99.99%) were weighed according to the stoichiometric ratio. Individual batches of 10 g were weighted according to the designed stoichiometry and mixed homogeneously with the same mass of absolute ethyl alcohol as the dispersant. After planetary ball-milling process, the obtained homogeneous slurry was placed in a Petri dish and dried in an oven. Then, the dried mixtures were put into a crucible with a lid and heated in a tubular furnace at 1250 °C for 6 hours under a reducing atmosphere of 5% H_2/95% N_2. When cooled down to room temperature, the prepared phosphors were crushed and ground for subsequent measurements.

2.2 Characterization

All crystal structure compositions were checked for phase formation by using powder X-ray diffraction (XRD) analysis with a Rigaku X-ray diffractometer (Tokyo, Japan) with a graphite monochromator using Cu Kα radiation ($\lambda = 1.54056$ Å), over the angular range $10 < 2\theta < 80$, operating at 40 kV and 40 mA. XRD Rietveld profile refinements of the structural models and textural analysis were performed with the use of TOPAS 4.2 software. The photoluminescence (PL) and photoluminescence excitation (PLE) spectra of the samples were analyzed by using a Hitachi F-7000 spectrophotometer (Tokyo, Japan) with a 150 W Xe lamp. The luminescence decay curve was obtained from a Lecroy Wave Runner 6100 digital oscilloscope (1 GHz) using a tunable laser (pulse width = 4 ns; gate = 50 ns) as the excitation source (Continuum Sunlite OPO). Optical properties such as luminescence spectra, correlated color temperature (CCT), color-rendering index, and the Commission International de l'Eclairage (CIE) color coordinates of the initial mixed phosphors and the white LEDs fabricated were characterized using a DARSA PRO 5100 PL system (PSI Trading Co. Ltd, Korea) and evaluated under a forward bias current of 60 mA at room temperature.

3. Results and discussion

3.1 Phase identification and crystal structure

Fig. 1(a) depicts powder XRD profiles of $Ca_{8-x}Sr_xMgGd(PO_4)_7$:-Eu^{2+} ($x = 0$, 1, 2, 3, 4, 5, 6, 7, and 8) samples along with the standard data $Ca_8MgGd(PO_4)_7$ (JCPDS card no. 50-1766). From Fig. 1, we can clearly find that all the diffraction peaks of the samples can be well indexed to the standard data of Ca_8-$MgGd(PO_4)_7$, which proves that the phase of $Ca_{8-x}Sr_x$-$MgGd(PO_4)_7$:Eu^{2+} samples is pure. $Ca_{8-x}Sr_xMgGd(PO_4)_7$:Eu^{2+} are isostructural with $Ca_8MgGd(PO_4)_7$ and the doping of Eu^{2+} ions does not cause significant impurities to the crystal structure. Fig. 1(b) shows the zoomed powder XRD profiles in the range of 29–32 degree, which exhibits the linear shift of peaks with the Ca replaced the Sr in $Ca_{8-x}Sr_xMgGd(PO_4)_7$:Eu^{2+} samples.

The lattice parameters from Rietveld refinements using TOPAS 4.2 are displayed in Fig. 2. The lattice parameters and

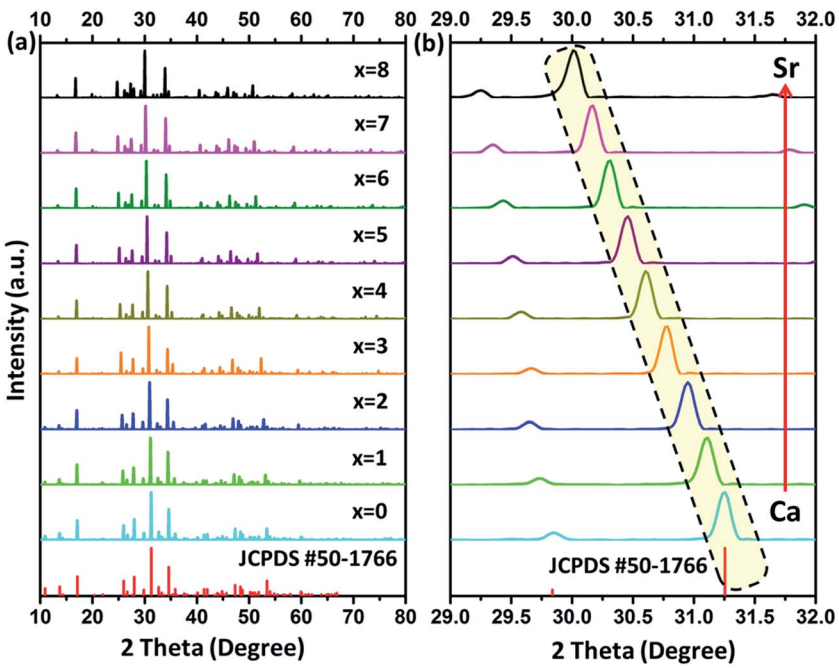

Fig. 1 (a) Representative powder XRD profiles of $Ca_{8-x}Sr_xMgGd(PO_4)_7$:Eu^{2+} ($x = 0$, 1, 2, 3, 4, 5, 6, 7, and 8) together with the standard data of $Ca_8MgGd(PO_4)_7$ (JCPDS card no. 50-1766). (b) The zoomed powder XRD profiles in the range of 29–32 degree.

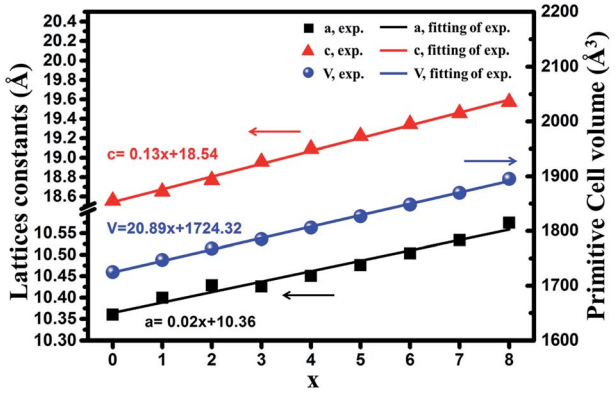

Fig. 2 Dependence of the measured lattice constants (*a* and *c*) and primitive cell volume (*V*) on *x* of the compounds $Ca_{8-x}Sr_xMgGd(PO_4)_7$ (x = 0, 1, 2, 3, 4, 5, 6, 7, 8).

cell volumes show a linear dependence on *x*, as can be anticipated from Vegard's law.[13] Moreover; the substitution is accompanied by a increase of *a*, *c* and *V*. The corresponding equations of the cell parameters as a function of chemical composition, *x*, are presented in Fig. 2 and can be explained by the difference in ionic radii between the substituted and substituting ions. It can been seen that both the lattice constants and primitive volume increase linearly when *x* increases in $Ca_{8-x}Sr_xMgGd(PO_4)_7$, which could be ascribed to the smaller ionic radius of Ca^{2+} ions (1.00 Å 1.12 Å and 1.18 Å when corresponding number is 6, 8 and 9, respectively) compared to that of Sr^{2+} ions (1.18 Å 1.26 Å and 1.31 Å when corresponding number is 6, 8 and 9, respectively).

To get the detailed crystal structure information on the obtained samples, we carried out Rietveld refinement of $Sr_8MgGd(PO_4)_7$:0.02Eu^{2+} sample with the single crystal structure data of $Sr_9MgH(PO_4)_7$ (ICSD no. 5113) as the initial model. Fig. 3 shows the observed (crosses) and calculated (red dots) XRD

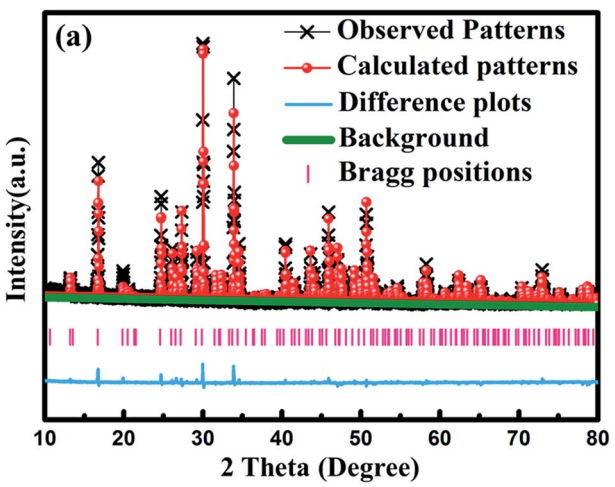

Fig. 3 Observed (crosses) and calculated (red dots) powder XRD patterns of $Sr_8MgGd(PO_4)_7$:0.02Eu^{2+} phosphor. The pink sticks stand for the positions of Bragg reflection and the blue line marks the difference between observed and calculated data.

Table 1 Rietveld refinement and crystallographic data of $Sr_8MgGd(PO_4)_7$:0.02Eu^{2+} sample

Formula	$Sr_8MgGd(PO_4)_7$:0.02Eu^{2+}
Space group	$R\bar{3}m$ (no. 166), trigonal
$a = b$ (Å)	10.569
c (Å)	19.57
$\alpha = \beta$ (deg)	90
γ (deg)	120
V (Å^3)	1893.22
R_p (%)	7.7
R_{wp} (%)	11.09
GOF	2.37

patterns together with their difference (blue) for the refinement of $Sr_8MgGd(PO_4)_7$:0.02Eu^{2+} sample. The refinement results reveal that $Sr_8MgGd(PO_4)_7$ has the trigonal structure with the space group of $R3m$, cell parameters of $a = b = 10.569$ Å, $c = 19.57$ Å, and cell volume of $V = 1893.22$ Å^3. And the refinement finally converged to GOF = 2.37, $R_p = 7.7\%$, and $R_{wp} = 11.09\%$ (Table 1), which again demonstrates that $Sr_8MgGd(PO_4)_7$ is isotypic with $Sr_9MgH(PO_4)_7$ and Eu^{2+} ions have been doped into the host lattice successfully.

The crystal structure model of $Sr_9MgH(PO_4)_7$ is depicted in Fig. 4. In the unit cell of $Sr_8MgGd(PO_4)_7$, there are three Sr crystallographic sites (Sr1, Sr2, and Sr3), two Mg sites (Mg1 and Mg2) and two P sites (P1 and P2). The coordinated polyhedrons of Sr1, Sr2 and Sr3 are also shown in Fig. 4.

3.2 Photoluminescence properties of $Ca_{8-x}Sr_xMgGd(PO_4)_7$:0.02Eu^{2+} doped phosphors

Fig. 5 shows PLE spectra of $Ca_{8-x}Sr_xMgGd(PO_4)_7$:0.02Eu^{2+} (x = 0, 1, 2, 3, 4, 5, 6, 7, 8). The excitation spectra monitored at 510 nm consist of broad bands ranging from 220–500 nm with a maximum at ~350 nm, which are assigned to $4f^7$–$4f^65d^1$

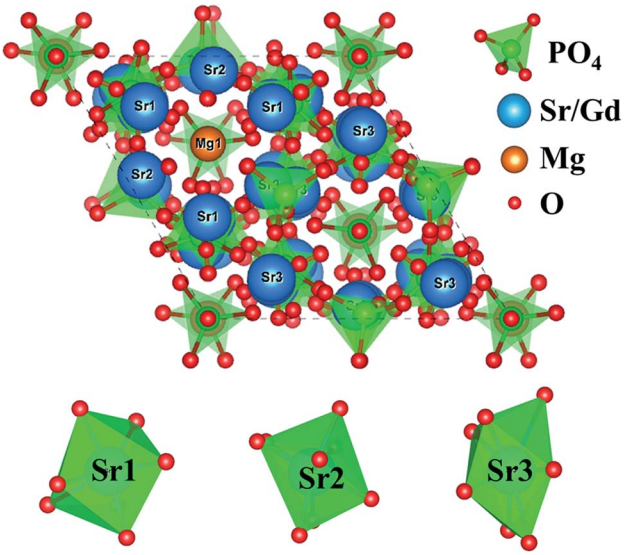

Fig. 4 Crystal structure of $Sr_8MgGd(PO_4)_7$ and the coordinated polyhedrons of Sr1, Sr2, Sr3.

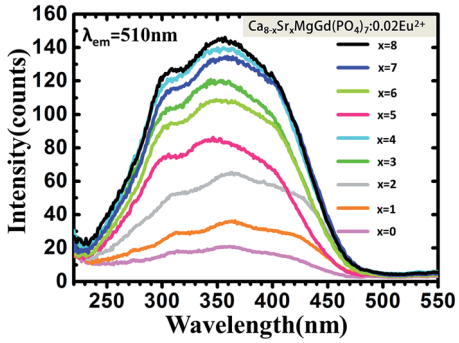

Fig. 5 PLE spectra of $Ca_{8-x}Sr_xMgGd(PO_4)_7$:0.02Eu^{2+} (x = 0, 1, 2, 3, 4, 5, 6, 7, 8).

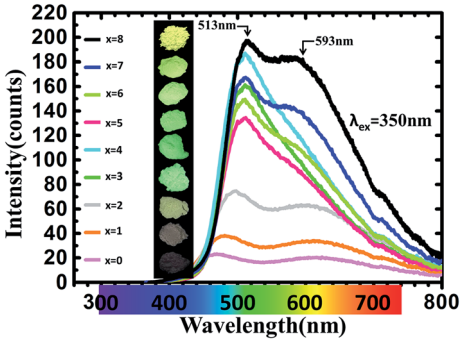

Fig. 6 PL spectra of $Ca_{8-x}Sr_xMgGd(PO_4)_7$:0.02Eu^{2+} (x = 0, 1, 2, 3, 4, 5, 6, 7, 8). The insets show photographs of phosphors excited by 365 nm excitation.

transition of Eu^{2+} ions. The PLE spectra nearly cover the region from UV to blue. Moreover, the PL spectra, as shown in Fig. 6, are measured and studied to further analyze the Eu^{2+} emitting centers in $Ca_{8-x}Sr_xMgGd(PO_4)_7$:0.02Eu^{2+}. The luminous intensity of $Ca_{8-x}Sr_xMgGd(PO_4)_7$:0.02Eu^{2+} is rather low when $x \leq 2$ for the difference between radius of Ca^{2+} (1 Å when corresponding number is 6) and that of Eu^{2+} (1.17 Å when corresponding number is 6) is very large. Then the luminous intensity increased with more Sr^{2+} replacing Ca^{2+}. The radius of Sr^{2+} (1.18 Å when corresponding number is 6) is very similar to the radius of Eu^{2+}, which leads the Eu^{2+} is easier to replace Sr^{2+} than Ca^{2+}. Interestingly, the two emission bands turn to one emission bands at green light region when x = 4, namely, $Ca_4Sr_4MgGd(PO_4)_7$:0.02Eu^{2+}. Form Fig. 2, it is known that both the lattices constants and primitive volume increase linearly when x increases in $Ca_{8-x}Sr_xMgGd(PO_4)_7$ which could be ascribed to the larger ionic radius of Sr^{2+} ions compared to that of Ca^{2+} ions. Eu^{2+} ions are easier to replace Sr^{2+} rather than Ca^{2+} because of their similar ionic radius. In $Ca_8MgGd(PO_4)_7$ host, Eu^{2+} is very difficult to replace Ca^{2+}, leading the weak emission intensity. Sr^{2+} makes the crystal lattice larger when Ca^{2+} is replaced by Sr^{2+}, which leading that Eu^{2+} can be easily doped into host, then the emission intensity increased. However, Eu^{2+} has the tendency to replace the Sr^{2+} which has similar ion radius in different Sr sites. So there are significant spectral variations when Ca^{2+} is subtitled by Sr^{2+}. When Sr^{2+} continues to replace Ca^{2+}, the green emission band turns back into two emission bands, covered with green and yellow regions. The insets show the photographs of phosphors excited by 365 nm excitation. From Fig. 7(a), fitted curve (red dashed line) and deconvoluted Gaussian components (red, green and blue dashed lines for peak 1, 2 and 3 respectively) of

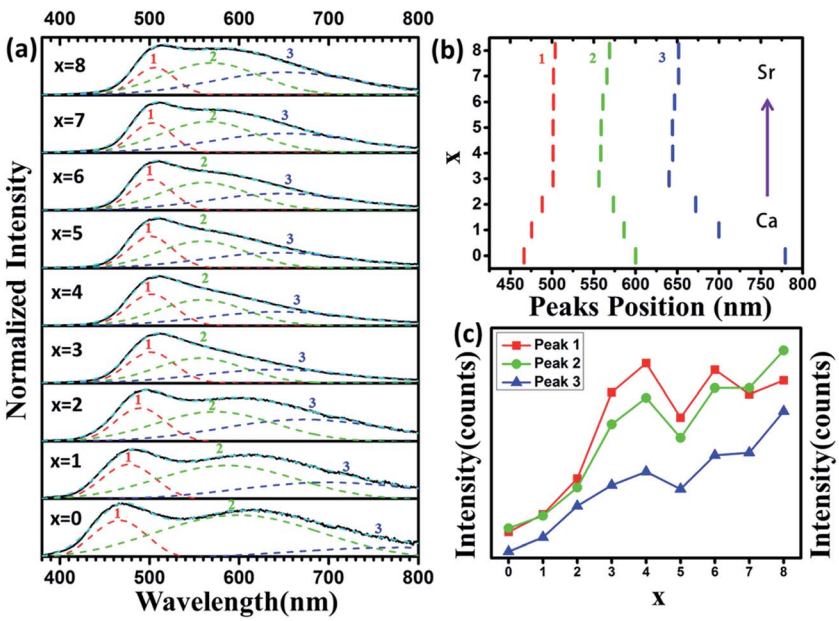

Fig. 7 (a) Fitted curve (red dashed line) and deconvoluted Gaussian components (red, green, blue and cyan dashed lines) of $Ca_{8-x}Sr_x$-$MgGd(PO_4)_7$:0.02Eu^{2+} (λ_{ex} = 350 nm). (b) The variation of peaks position with x increase in $Ca_{8-x}Sr_xMgGd(PO_4)_7$:0.02Eu^{2+} (x = 0, 1, 2, 3, 4, 5, 6, 7, 8). (c) The comparison of peaks intensity.

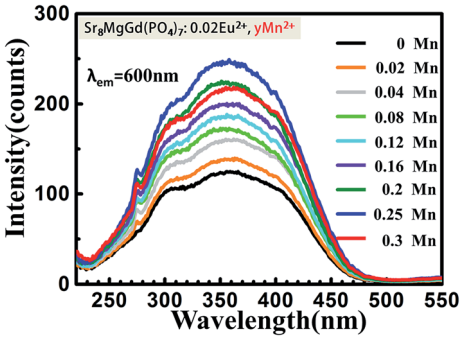

Fig. 8 PLE spectra of $Sr_8MgGd(PO_4)_7:Eu^{2+},yMn^{2+}$ (y = 0, 0.02, 0.04, 0.08, 0.12, 0.16, 0.2, 0.25).

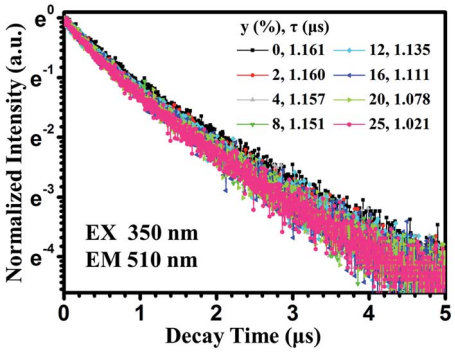

Fig. 10 PL decay curves of Eu^{2+} in $Sr_8MgGd(PO_4)_7:Eu^{2+},yMn^{2+}$ (excited at 350 nm and monitored at 510 nm).

$Ca_{8-x}Sr_xMgGd(PO_4)_7:0.02Eu^{2+}$ (λ_{ex} = 350 nm) are shown in detail. It can be seen that there are three deconvoluted Gaussian peaks of Eu^{2+} corresponding to three types of Sr^{2+}/Ca^{2+} sites in all samples. Peak 1 has a red shift before $x = 4$, while peak 2 and peak 3 have a blue shift before $x = 4$ with the increase replacement of Sr^{2+}, which is shown in Fig. 7(b). However, the emission peak position would not change when $x > 4$, which means the luminescence of Eu^{2+} no longer depends strongly on the change of crystal field, even though the lattice parameters still increase. As depicted in Fig. 7(c), the luminous intensity increased and reached maximum at $x = 4$, and then decreased. After $x = 6$, the luminous intensity increased again and reached maximum at $x = 8$, that is $Sr_8MgGd(PO_4)_7:0.02Eu^{2+}$.

3.3 Energy transfer properties in $Sr_8MgGd(PO_4)_7:Eu^{2+},Mn^{2+}$ phosphors

The PLE spectra (Fig. 8.) increase the intensity with increasing the concentration of doping Mn^{2+} ions when monitored at 600 nm. The broad excitation bands covered from 220 nm to 470 nm. Under the excitation of 350 nm, both the emission of Eu^{2+} and Mn^{2+} can be observed in the PL spectrum of the co-doped samples as shown in Fig. 9. The emission intensity for Eu^{2+} decreases with increasing Mn^{2+} concentration, whereas the emission intensity for Mn^{2+} increases with increasing the concentration. The insets show photographs of phosphors excited by 365 nm excitation. The color turns from yellow to orange-yellow with the increasing Mn^{2+} concentration. There is a concentration quenching about Mn^{2+} 616 nm emission peak when $y > 0.25$ in $Sr_8MgGd(PO_4)_7:0.02Eu^{2+},yMn^{2+}$.

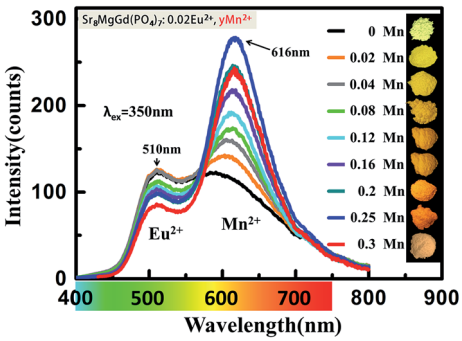

Fig. 9 PL spectra of $Sr_8MgGd(PO_4)_7:0.02Eu^{2+},yMn^{2+}$ (y = 0, 0.02, 0.04, 0.08, 0.12, 0.16, 0.2, 0.25). The insets show photographs of phosphors excited by 365 nm excitation.

In order to well understand the energy transfer process, we measured the PL decay curves and then calculated the lifetimes as well as energy-transfer efficiencies. Fig. 10 shows the PL decay curves of the Eu^{2+} ions in $Sr_8MgGd(PO_4)_7:Eu^{2+},yMn^{2+}$, which were measured with excitation at 350 nm and monitored at 510 nm. One can see that the decay curve of the singly Eu^{2+} doped $Sr_8MgGd(PO_4)_7:Eu^{2+}$ sample can be well fitted into a single-exponential function with a decay time of 1.161 μs. This is the radiative decay time of the Eu^{2+} ions. For the Eu^{2+} and Mn^{2+} codoped samples, the doping of the Mn^{2+} ions significantly modifies the fluorescent dynamics of the Eu^{2+} ions. The results reveal that the fluorescence decays deviate slightly from a single exponential rule, indicating the presence of a non-radiative process. The effective lifetime is defined as

$$\tau = \frac{\int_0^\infty tI(t)\mathrm{d}t}{\int_0^\infty I(t)\mathrm{d}t} \quad (1)$$

On the basis of eqn (1), the effective lifetime values were calculated to be 1.160, 1.157, 1.151, 1.135, 1.111, 1.078, and 1.021 μs for $Sr_8MgGd(PO_4)_7:Eu^{2+},yMn^{2+}$ with $y = 0.02$, 0.04, 0.08, 0.12, 0.16, 0.2, and 0.25, respectively. It can be seen that the decay lifetime of the Eu^{2+} ions decreases monotonically with an increase in the Mn^{2+} doping concentration, which strongly supports energy transfer from the Eu^{2+} to Mn^{2+} ions.

Based on the following equation,[14] the energy transfer efficiency (η_T) from Eu^{2+} to Mn^{2+} can be evaluated:

$$\eta_T = 1 - \frac{\tau_s}{\tau_{so}} \quad (2)$$

where τ_s and τ_{so} are the decay time of the Eu^{2+} ions in the absence and presence of Mn^{2+} ions.

The results are shown in Fig. 11. It can be observed that the η_T increases gradually with the increase of the Mn^{2+} doping concentration and finally reaches to 0.12 for $y = 0.25$.

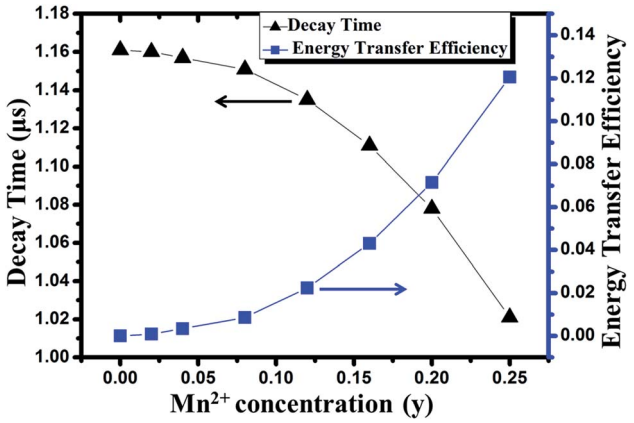

Fig. 11 Dependence of decay time and energy transfer efficiency on the concentration of Mn^{2+} in $Sr_8MgGd(PO_4)_7:Eu^{2+},yMn^{2+}$ phosphor.

According to Dexter's theory,[15] non-radiative energy transfer between sensitizer and activator ions can occur by exchange interaction, or multipolar interactions. The following formula will be fitted linearly if exchange interaction works:

$$\ln\frac{\eta_{so}}{\eta_s} \propto C \quad (3)$$

where C is the total concentration of Eu^{2+} and Mn^{2+} ions, η_{so} and η_s are the luminescence quantum efficiencies of Eu^{2+} in the absence and presence of Mn^{2+}, respectively. The value of η_{so}/η_s can be approximately estimated from the related decay time's ratio τ_{so}/τ_s. Thus, eqn (3) can be represented by the following equation:

$$\ln\frac{\tau_{so}}{\tau_s} \propto C \quad (4)$$

As shown in Fig. 12(a), linear relation is not well obtained *via* exchange interaction ($R^2 = 0.858$). Therefore, the energy of Eu^{2+} is transferred to Mn^{2+} by multiple–multiple interaction. For multipolar interactions, the following relation can be obtained:

$$\frac{\eta_{so}}{\eta_s} \propto C^{\alpha/3} \quad (5)$$

As mentioned above, eqn (5) can be also represented by the following equation:

$$\frac{\tau_{so}}{\tau_s} \propto C^{\alpha/3} \quad (6)$$

where $a = 6$, 8 and 10 is corresponding to dipole–dipole, dipole–quadrupole and quadrupole–quadrupole interactions, respectively. In Fig. 12(b)–(d), it can be observed that a well fitted linear relation was obtained when $a = 8$, which indicates that the dominant interaction mechanism for energy transfer from Eu^{2+} to Mn^{2+} in $Sr_8MgGd(PO_4)_7$ is dipole–quadrupole interaction.

3.4 Temperature-dependent emission spectra, LED lamp fabrication and EL spectrum

To demonstrate the potential application of $Ca_{8-x}Sr_xMgGd(PO_4)_7:0.02Eu^{2+}$ and $Sr_8MgGd(PO_4)_7:0.02Eu^{2+},yMn^{2+}$ phosphor, as shown in Fig. 13, temperature-dependent integrated PL intensity of the phosphors have been obtained. These three types of

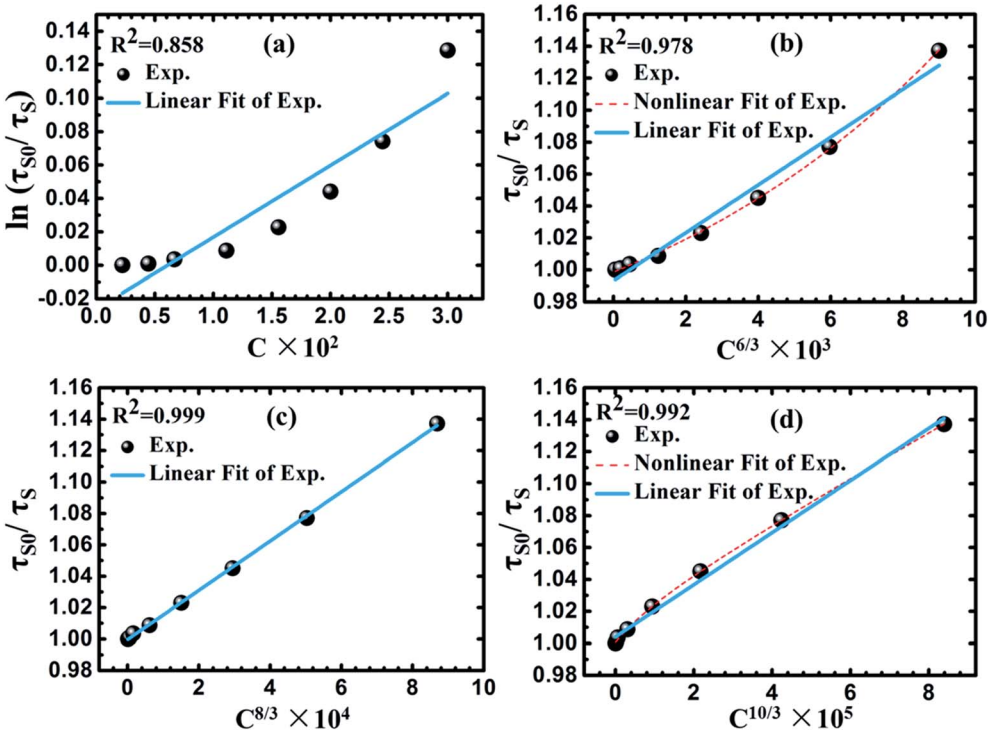

Fig. 12 Dependence of $\ln(\tau_{so}/\tau_s)$ of Eu^{2+} on C_{Eu+Mn} (a), and τ_{so}/τ_s of Eu^{2+} on $C^{6/3}$ (b), $C^{8/3}$ (c) and $C^{10/3}$ (d).

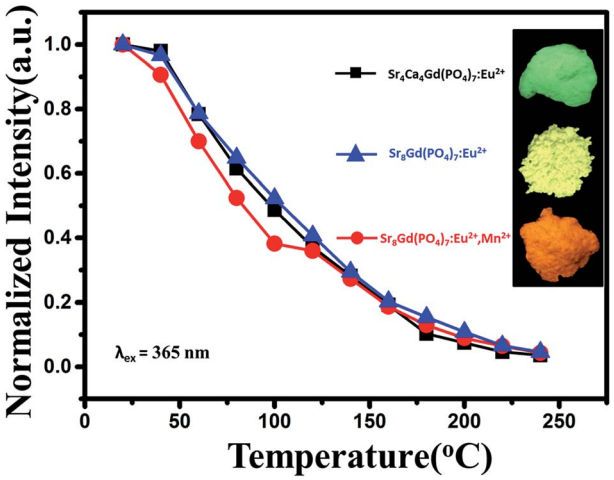

Fig. 13 Temperature-dependent integrated PL intensity of $Sr_4Ca_4Gd(PO_4)_7$:0.02Eu^{2+}, $Sr_8Gd(PO_4)_7$:0.02Eu^{2+} and $Sr_8Gd(PO_4)_7$:0.02Eu^{2+},0.25Mn^{2+} phosphors. Inset: photographs of the phosphors under 365 nm UV-light.

phosphors have similar thermal stabilities. There is around 50% intensity attenuation when temperature is 100 °C. The internal quantum efficiency of $Sr_4Ca_4Gd(PO_4)_7$:0.02Eu^{2+}, $Sr_8Gd(PO_4)_7$:0.02Eu^{2+} and $Sr_8Gd(PO_4)_7$:0.02Eu^{2+},0.25Mn^{2+} phosphors is 20.6%, 30.2% and 17.8%. As Fig. 14(a) shows, phosphor-converted LED was fabricated by combining a 365 nm UV-chip and driven by a forward-bias current of 60 mA. Point B, G, Y, O and R represent $Sr_5(PO_4)_3Cl$:0.02Eu^{2+} blue phosphor, $Ca_4Sr_4MgGd(PO_4)_7$:0.02Eu^{2+} green phosphor, $Sr_8MgGd(PO_4)_7$:0.02Eu^{2+} yellow phosphor, $Sr_8MgGd(PO_4)_7$:0.02Eu^{2+},0.25Mn^{2+} orange phosphor and $Sr_4Al_{14}O_{25}$:0.01Mn^{4+} red phosphor, respectively. All the possible that mixed kinds of phosphors are contained in the area of dashed triangle. BGR (or BYR) represents the mixture composed of $Sr_5(PO_4)_3Cl$:0.02Eu^{2+} blue phosphor, $Sr_4Al_{14}O_{25}$:0.01Mn^{4+} red phosphor and $Ca_4Sr_4MgGd(PO_4)_7$:0.02Eu^{2+} green phosphor (or $Sr_8MgGd(PO_4)_7$:0.02Eu^{2+} yellow phosphor). A standard warm white-light emitting single-phased phosphor of $Sr_8MgGd(PO_4)_7$:Eu^{2+},Mn^{2+} (point O) with chromaticity coordinates (x, y), correlated color temperature (CCT) and Commission Internationale de l'Eclairage (CIE) coordinates of ((0.4497, 0.3929), 2705 K, 89.7) is realized *via* energy transfer between Eu^{2+} and Mn^{2+}. The insets show photographs of the LED lamp packages driven by 60 mA current. Fig. 14(b) and (c) show the electroluminescence (EL) spectra of the lamps. Three emission bands can be clearly seen in Fig. 14(b): 450 nm, attributed to $Sr_5(PO_4)_3Cl$:0.02Eu^{2+} blue phosphor, the 510 and 668 nm, attributable to the $Ca_4Sr_4MgGd(PO_4)_7$:0.02Eu^{2+} green phosphor and $Sr_4Al_{14}O_{25}$:0.01Mn^{4+} red phosphor, respectively. CRI value of BGR is 94.1 and CCT is 7556 K. Four emission bands can be clearly seen in Fig. 14(c), 450 nm, attributed to $Sr_5(PO_4)_3Cl$:0.02Eu^{2+} blue phosphor, the 510 and 600 nm, attributable to the $Sr_8MgGd(PO_4)_7$:0.02Eu^{2+} yellow phosphor, $Sr_4Al_{14}O_{25}$:0.01Mn^{4+} red phosphor, respectively. CRI value of BYR reach up to 97 and CCT is 5651 K. The luminous efficiencies of BGR, BYR and O LED prototype under 60 mA are 23.67 lm W^{-1}, 24.03 lm W^{-1} and 24.28 lm W^{-1}, respectively. The low luminous efficiency contributes to our low efficient 365 nm UV-chips. The CIE chromaticity diagram, CIE chromaticity coordinates, CCT, and R_a were listed in Table 2. The results obtained for the LED package demonstrated that

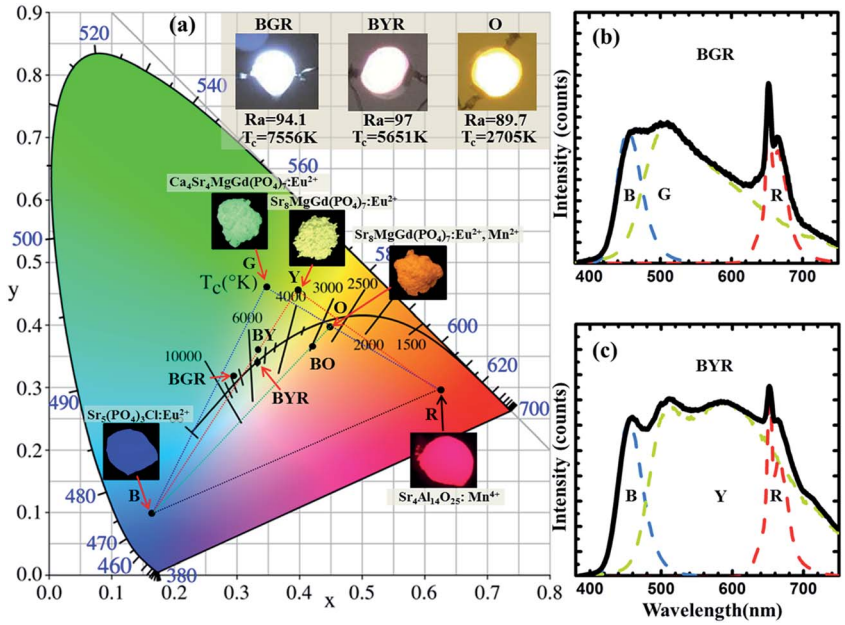

Fig. 14 CIE chromaticity diagram of a mixing of $Ca_4Sr_4MgGd(PO_4)_7$:0.02Eu^{2+} green phosphors (point G), $Sr_8MgGd(PO_4)_7$:0.02Eu^{2+} yellow phosphors (point Y), $Sr_8MgGd(PO_4)_7$:0.02Eu^{2+},0.25Mn^{2+} orange phosphors (point O), $Sr_5(PO_4)_3Cl$:0.02Eu^{2+} blue phosphors (point B) and $Sr_4Al_{14}O_{25}$:0.01Mn^{4+} red phosphors (point R). The insets show photographs of LED package with 365 nm UV-chips driven by 60 mA current and phosphors excited by 365 nm excitation.

Table 2 CIE chromaticity coordinates, CCT, and R_a for marked points

Point	Components	(x, y)	CCT (K)	R_a
B	$Sr_5(PO_4)_3Cl$:0.02Eu^{2+}	(0.1641, 0.0994)	—	18.3
G	$Ca_4Sr_4MgGd(PO_4)_7$:0.02Eu^{2+}	(0.3492, 0.4599)	5125	72.0
Y	$Sr_8MgGd(PO_4)_7$:0.02Eu^{2+}	(0.3972, 0.4535)	4080	82.0
O	$Sr_8MgGd(PO_4)_7$:0.02Eu^{2+},0.25Mn^{2+}	(0.4497, 0.3929)	2705	89.7
R	$Sr_4Al_{14}O_{25}$:0.01Mn^{4+}	(0.6252, 0.2859)	1001	20.6
BY	B + Y	(0.3316, 0.3719)	5541	90.3
BO	B + O	(0.4155, 0.3548)	2949	84.9
BGR	B + G + R	(0.2966, 0.3213)	7556	94.1
BYR	B + Y + R	(0.3290, 0.3410)	5651	97.0

$Ca_{8-x}Sr_xMgGd(PO_4)_7$:0.02Eu^{2+} has potential applications in the full-spectrum white-light NUV LEDs with excellent CRIs.

4. Conclusions

In summary, we have synthesized two series of novel phosphors of $Ca_{8-x}Sr_xMgGd(PO_4)_7$:Eu^{2+} and $Sr_8MgGd(PO_4)_7$:Eu^{2+},yMn^{2+} by the high temperature solid-state reaction. A warm white-light emitting single-phased phosphor of $Sr_8MgGd(PO_4)_7$:Eu^{2+},Mn^{2+} with chromaticity coordinates (x, y), correlated color temperature (CCT) and Commission Internationale de l'Eclairage (CIE) coordinates of ((0.4497, 0.3929), 2705 K, 89.7) is realized *via* energy transfer between Eu^{2+} and Mn^{2+}. The energy transfer was demonstrated to be a resonant type dipole–quadrupole mechanism. A white LED with $R_a = 97$ (or $R_a = 94.1$) was successfully fabricated by coating $Sr_8MgGd(PO_4)_7$:Eu^{2+} (or $Ca_4Sr_4MgGd(PO_4)_7$:Eu^{2+}) with a blend of $Sr_5(PO_4)_3Cl$:Eu^{2+} blue and $Sr_4Al_{14}O_{25}$:Mn^{4+} red phosphor onto a near UV 365 nm chip.

Acknowledgements

This work was financially supported by the programs of National Natural Science Foundation of China (No. 51272282 & 51302311), and significant achievement transformation project of colleges and universities of the Central in Beijing (ZD20141000201), supported by Beijing Municipal Education Commission.

References

1 S. Nakamura, T. Mukai and M. Senoh, Candela. Candela-class high-brightness InGaN/AlGaN double-heterostructure blue-light-emitting diodes, *Appl. Phys. Lett.*, 1994, **64**, 1687–1689.

2 P. Thiyagarajan, M. Kottaisamy and M. S. Ramachandra Rao, Luminescent properties of near UV excitable Ba_2ZnS_3:Mn red emitting phosphor blend for white LED and display applications, *J. Phys. D: Appl. Phys.*, 2006, **39**, 2701–2706.

3 V. Bachmann, C. Ronda and A. Meijerink, Temperature Quenching of Yellow Ce^{3+} Luminescence in YAG:Ce, *Chem. Mater.*, 2009, **21**, 2077–2084.

4 A. A. Setlur, W. J. Heward, Y. Gao, A. M. Srivastava, R. G. Chandran and M. V. Shankar, Crystal Chemistry and Luminescence of Ce^{3+}-Doped $Lu_2CaMg_2(Si,Ge)_3O_{12}$ and Its Use in LED Based Lighting, *Chem. Mater.*, 2006, **18**, 3314–3322.

5 H. S. Jang, Y. H. Won and D. Y. Jeon, Improvement of Electroluminescent Property of Blue LED Coated with Highly Luminescent Yellow-Emitting Phosphors, *Appl. Phys. B: Lasers Opt.*, 2009, **95**, 715–720.

6 L. Huang, M. Guo, S. Zhao, D. Deng, H. Wang, Y. Hua, G. Jia and S. Xu, Luminescence of Ca_2LiSiO_4F:Ce^{3+},Tb^{3+} Phosphors, *ECS J. Solid State Sci. Technol.*, 2013, **2**, R3083–R3087.

7 A. A. Setlur, W. J. Heward, Y. Gao, A. M. Srivastava, R. G. Chandran and M. V. Shankar, Crystal Chemistry and Luminescence of Ce^{3+}-Doped $Lu_2CaMg_2(Si,Ge)_3O_{12}$ and Its Use in LED Based Lighting, *Chem. Mater.*, 2006, **18**, 3314–3322.

8 N. Guo, Y. Huang, H. You, M. Yang, Y. Song, K. Liu and Y. Zheng, $Ca_9Lu(PO_4)_7$:Eu^{2+},Mn^{2+}: A Potential Single-Phased White-Light-Emitting Phosphor Suitable for White-Light-Emitting Diodes, *Inorg. Chem.*, 2010, **49**, 10907.

9 H. Yanlin, D. Haiyan, J. Kiwan, C. Eunjin, L. Ho, M. Jayasimhadri and Y. Soung-Soo, Luminescence properties of triple phosphate $Ca_8MgGd(PO_4)_7$:Eu^{2+} for white light-emitting diodes, *J. Phys. D: Appl. Phys.*, 2008, **41**, 095110.

10 C. H. Huang, D. Y. Wang, Y. C. Chiu, Y. T. Yeh and T. M. Chen, $Sr_8MgGd(PO_4)_7$:Eu^{2+}: yellow-emitting phosphor for application in near-ultraviolet-emitting diode based white-light LEDs, *RSC Adv.*, 2012, **2**, 9130–9134.

11 W. Z. Sun, Y. L. Jia, R. Pang, H. F. Li, T. F. Ma, J. P. Fu, S. Zhang and L. H. Jiang, $Sr_9Mg_{1.5}(PO_4)_7$:Eu^{2+}: A Novel Broadband Orange-Yellow-Emitting Phosphor for Blue Light-Excited Warm White LEDs, *ACS Appl. Mater. Interfaces*, 2015, **7**, 25219–25226.

12 D. Wen, Z. Dong, J. Shi, M. Gong and M. Wu, Standard White-Emitting $Ca_8MgY(PO_4)_7$:Eu^{2+},Mn^{2+} Phosphor for White-Light-Emitting LEDs, *ECS J. Solid State Sci. Technol.*, 2013, **2**, R178–R185.

13 A. R. Denton and N. W. Ashcroft, Vegard's law, *Phys. Rev. A: At., Mol., Opt. Phys.*, 1991, **43**, 3161–3164.

14 P. I. Paulose, G. Jose, V. Thomas, N. V. Unnikrishnan and M. K. R. Warrier, Luminescence Properties of Mn^{2+}-Doped Sol–Gel Glasses, *J. Phys. Chem. Solids*, 2003, **64**, 841.

15 D. L. Dexter and J. A. Schulman, Theory of Concentration Quenching in Inorganic Phosphors, *J. Chem. Phys.*, 1954, **22**, 1063–1070.

